SUPPLEMENTARY MATERIAL

eMethods

Alzheimer's Disease Neuroimaging Initiative (ADNI)

Data used in this study were obtained from the Alzheimer's Disease Neuroimaging Initiative (ADNI) database (www.adni.loni.usc.edu). The ADNI was launched in 2003 as a public-private partnership, led by Principal Investigator Michael W. Weiner, MD. It is a longitudinal multi-phase, multi-center study to develop clinical, imaging, genetic, and biochemical biomarkers for early detection and measuring AD progression. Up-to-date information on the various study phase protocols, assessments, and follow-up duration are available on www.adni-info.org.

Image preprocessing and constructing WMH probability maps

Image analysis was performed using 2D FLAIR and T1-weighted brain MRIs to construct WMH probability maps for each participant using the following steps: (i) we applied the brain segmentation tool from Statistical Parametric Mapping (SPM12)[1] to the T1-weighted scans to segment the head region from the background, removing non-brain tissues; (ii) the resulting brain masks were co-registered to corresponding FLAIR images using the FLIRT tool[2] in the FSL Toolbox (FMRIB, Oxford, UK)[3] to enable skull-stripping; (iii) bias field correction was performed using the FAST tool[4] in FSL; (iv) brain intensities within each FLAIR image were normalized using a modified Z-score transformation with 2*SD for intensity standardization across participant images. We visually checked all pre-processed data after each analytical step for quality control to rule out inaccurate preprocessing results; (v) we utilized an automated method for voxel-level localization and accurate quantification of WMH from 2D FLAIR images using a deep neural network based on the U-Net architecture[5]. For each participant, the trained in-house deep-learning network takes the intensity-normalized axial FLAIR image of a size 256 x 256 as input, and constructs a participant-specific 2D WMH probability maps that provide probabilistic information about voxel-wise WMH distribution; (vi) individual 2D WMH probability maps were co-registered to their corresponding T1-weighted images to spatially align image pairs using a 12-parameter affine registration with FLIRT[2]; (vii) finally, we used nonlinear

registration implemented in Advanced Normalization Tools[6] for warping to a common ICBM-152 brain template (http://nist.mni.mcgill.ca/icbm-152-nonlinear-atlases-2009/), generating participant-specific 3D WMH probability maps that served as inputs for the subsequent voxel-wise spectral clustering analysis.

Deep learning network for automated WMH segmentation

The U-Net is a CNN architecture that implements a dual pathway, deep encoder-decoder scheme with skip connections concatenating the feature maps in the encoder to the feature maps in the decoder, to learn both context (contracting path) and precise spatial location (expansion path). Variants of the standard U-Net architecture more consistently demonstrated better performance in WMH segmentation compared with other methods.[7,8] We adopted the standard U-Net configurations including 3 x 3 kernel convolutions with a rectified linear unit (ReLU) as activation function and batch normalization after each convolution (**eFigure 1**). The contracting path had two 2 x 2 max-pooling operations after every two convolution layers (stride=2 for down-sampling) that reduce the spatial dimensions while doubling the number of feature channels, whereas up-sampling layers based on nearest-neighbor interpolation were applied after every two convolutional layers in the expansion path. Feature maps were also concatenated with corresponding feature maps from the contracting path prior to down-sampling. At the final layer, a 1 x 1 convolution with softmax function was used to convert the feature maps into an output space with two classes (WMH and non-WMH).

Network training and validation were performed on a GeForce GTX 1080 Ti GPU card. 2D FLAIR axial slices (256 x 256 x 1) were fed into a single channel as input using the Adam optimizer with cross-entropy cost as the loss function, and a mini-batch size of 20. The learning rate was initialized at 10^{-4} and dropout rate was set to 0.2. In the training step, we performed 5-fold cross-validation where each fold (n=10) images were randomly sampled from the whole training set (n=50) and retained as validation data for model testing, with the remaining four folds (n=40) used for training the proposed network. This process was iterated 5 times, resulting in 5 separately trained networks. For testing, we used images from our test dataset (n=20) as input to each network generated from the 5-

fold cross-validation for independent testing, and the resulting outputs from the five networks were averaged to produce the final output.

Evaluation of automated WMH segmentation

We validated our method using 70 ADNI participant images selected at random, blind from any clinical, imaging, or demographic information at the time of selection. These image samples were randomly divided into a training dataset (n=50) and test dataset (n=20). We created a reference standard for supratentorial WMH by performing manual WMH segmentation in accordance with the STRIVE criteria.[9] Using a contour drawing technique, a trained clinician (R1) with extensive experience in lesion segmentation delineated WMH manually on the 2D multi-slice FLAIR images in both training and test datasets using MRIcron software by tracing the WMH outline with a mouse-controlled interface. This process resulted in creation of binary masks, whereby all voxels within the manual delineation were considered WMH (label 1), with remaining voxels as background (label 0). To assess inter-rater reliability of the reference segmentations, 20 of the manual delineations were randomly selected for peer-review and separately delineated by a second expert (R2) with >5 years of experience in quantitative neuroimaging, blinded to previous assessments.

We evaluated WMH segmentation performance by comparing WMH segmentation maps generated by our proposed deep network (DL) with the reference manual WMH segmentation maps (MN) in our independent test dataset (n=20) using a set of evaluation metrics: (i) DSC, an overlap index measuring the similarity or spatial coincidence between MN and DL results, (ii) volume difference (VD) between DL and MN WMH segmentation masks, (iii) area under the curve of precision-recall metrics (AUC-PR), (iv) a modified Housdorff distance (95^{th} percentrile; H95) as the overall distance between the DL and MN boundaries, (v) the absolute percentage volume difference (AVD) between the DL-segmented and MN-segmented WMH volumes, (vi) recall as the sensitivity in detecting individual lesions, and (vii) F1-score as the average of precision and recall in detecting individual lesions.

Constructing a lobar cerebral microbleed density map

We created location masks of strictly lobar cerebral microbleeds (SL-CMBs) for each participant by manual segmentation of SL-CMBs from T2*-weighted gradient-recalled echo (T2*-GRE) MRIs, defined according to consensus criteria[10] as hypointense lesions within gray or white matter in lobar brain regions that are distinct from iron or calcium deposits and vessel flow voids. A composite density map of SL-CMBs across participants was constructed by: (i) registering the SL-CMBs location masks to their corresponding T1-weighted image space using the *epi_reg* function within the FLIRT toolbox in FSL,[3] (ii) performing high-dimensional warping of the co-registered SL-CMBs location masks to a common ICBM-152 brain template using nonlinear registration in ANTs,[6] and (iii) averaging the spatially normalized SL-CMBs location masks to create a SL-CMBs frequency map across participants.

References

1. Statistical Parametric Mapping (SPM): http://www.fil.ion.ucl.ac.uk/spm/
2. Jenkinson M, Smith S. A global optimization method for robust affine registration of brain images. *Med Image Anal*. 2001;5:143-156
3. Smith SM, Jenkinson M, Woolrich MW, et al. Advances in functional and structural MR image analysis and implementation as FSL. *NeuroImage*. 2004;23(S1):208-219
4. Zhang Y, Brady M, Smith S. Segmentation of brain MR images through a hidden Markov random field model and the expectation-maximization algorithm. *IEEE Trans Med Imaging*.2001;20:45-57
5. Ronneberger O, Fischer P, Brox T. U-Net: Convolutional Networks for Biomedical Image Segmentation. *Medical Image Computing and Computer-Assisted Intervention (MICCAI)*. 2015; Springer, LNCS, 9351:234-241
6. Avants BB, Epstein CL, Grossman M, Gee JC. Symmetric diffeomorphic image registration with cross-correlation: evaluating automated labelling of elderly and neurodegenerative brain. Med. Image. Anal. 2008;12:26-41
7. Kuijf HJ, Casamitjana A, Collins LD, et al. Standardized Assessment of Automatic Segmentation of White Matter Hyperintensities and Results of the

WMH Segmentation Challenge. *IEEE Trans Med Imaging*. 2019;38 (11):2556-2568

8. Li H, Jiang G, Zhang J, et al. Fully convolutional network ensembles for white matter hyperintensities segmentation in MR images. *NeuroImage*. 2018;183:650-665
9. Wardlaw JM, Smith EE, Biessels GJ, et al. Neuroimaging standards for research into small vessel disease and its contribution to ageing and neurodegeneration. *Lancet Neurol*. 2013;12(8):822-838
10. Greenberg SM, Vernooij MW, Cordonnier C, et al. Cerebral microbleeds: a guide to detection and interpretation. *Lancet Neurol.* 2009;8:165-174

eFigure 1. CNN architecture for automated WMH segmentation

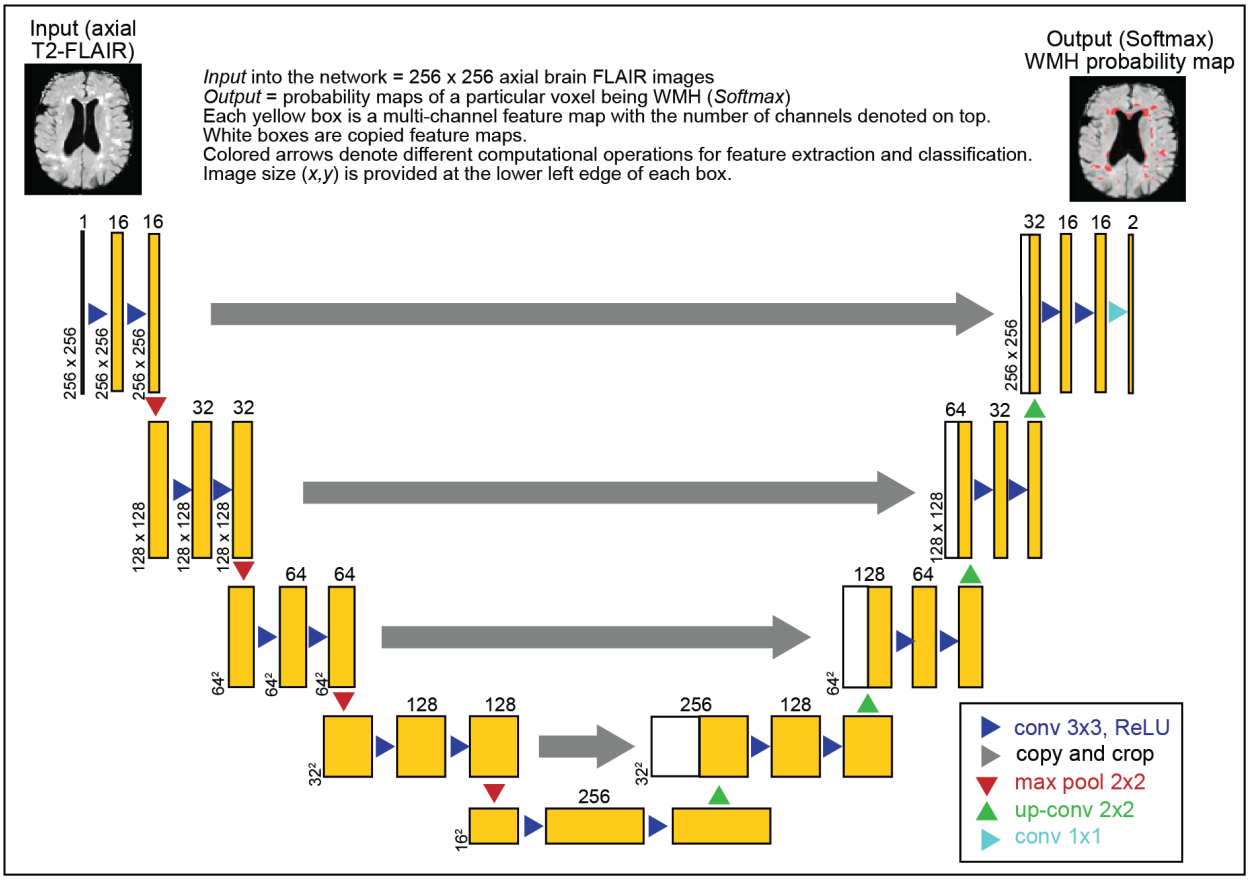

The U-Net architecture of the deep learning network for automated WMH segmentation is composed of a contracting path and an expansive path. The contracting path consist of repeated applications of two 3x3 padded convolutions, each followed by a rectified linear unit (ReLU) and a 2x2 max pooling operation with a stride of 2 for downsampling. Each step in the expanding path involve an upsampling of the feature map, a 2x2 convolution that halved the number of feature channels, concatenation of the feature map and two 3x3 convolutions, each followed by a ReLU. For the final layer, a 1x1 convolution maps each 64-component feature vector to two classes (WMH and non-WMH).

eFigure 2. Comparison of WMH segmentation accuracy measured by DSC and AUC-PR between U-Net and UCD Four Tissue automated segmentation schemes across different WMH burden.

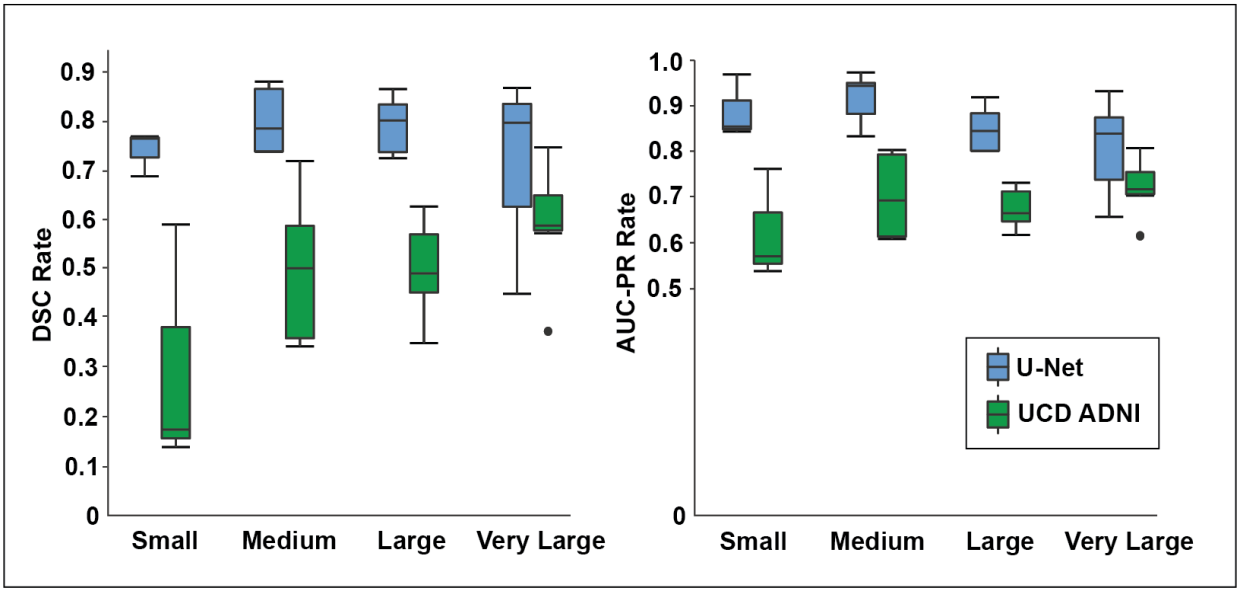

ADNI test dataset grouped by WMH burden (in cc, number of MRI data): Small (≤4.5; n= 3), Medium (>4.5 – ≤13; n= 5), Large (>13 – ≤24; n= 5), Very Large (>24, n= 7). The central line, top and bottom edges of each box plot represent the median, 25th and 75th percentiles, respectively; error bars extend to the most extreme non-outlier data points; outliers are indicated by the symbol • .

eFigure 3. Visualization of the automated WMH segmentation results from the U-Net and UCD Four Tissue segmentation schemes.

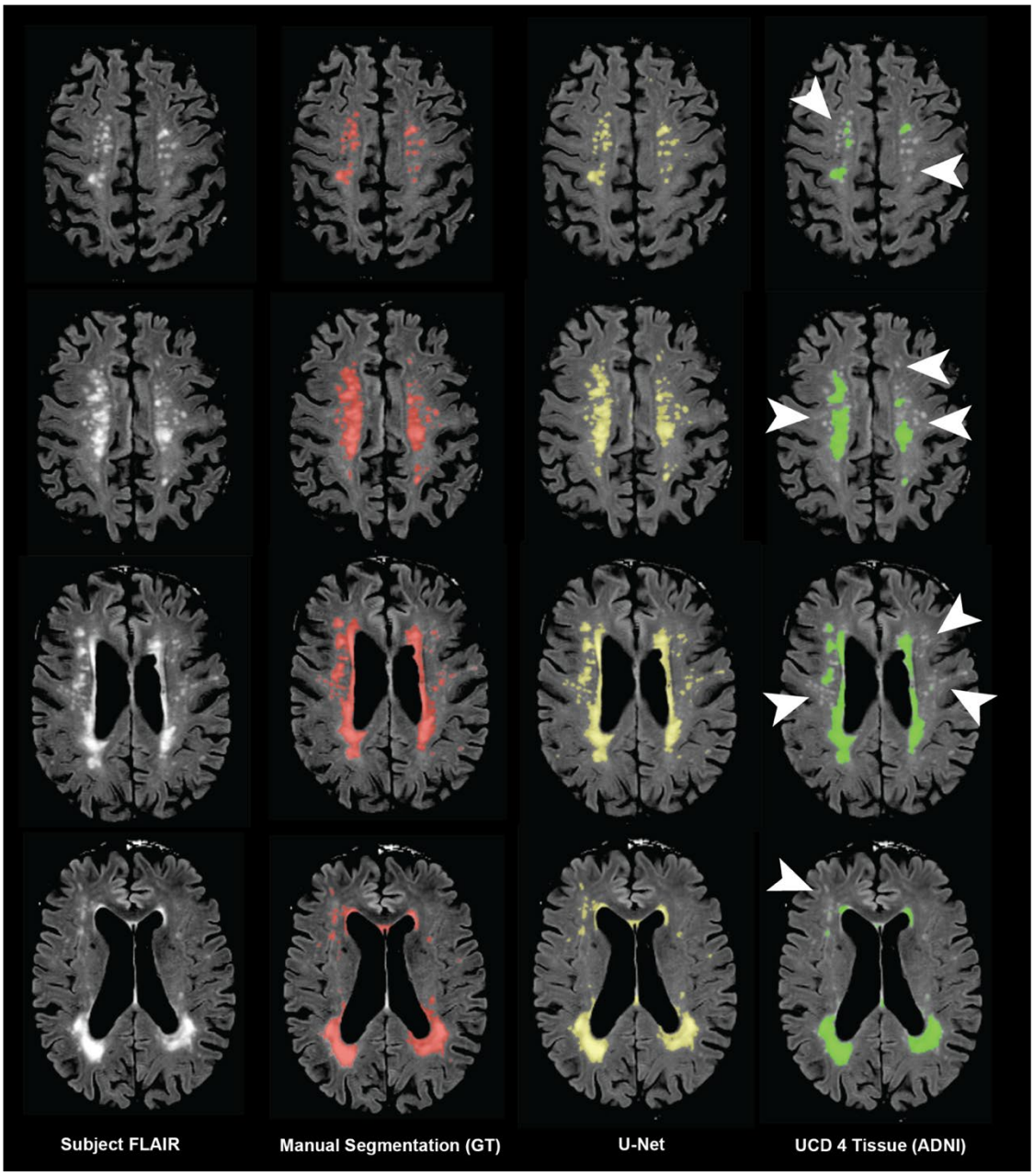

Regions in **red** are WMH labelled manually by experts (GT), regions in **yellow** are labelled by the deep learning-based (U-Net) algorithm, and regions in **green** are labelled by the UCD Four Tissue segmentation method. White arrows indicate WMH that were not identified by the UCD Four Tissue segmentation scheme (false negatives).

eFigure 4. Plot of eigenvalues of the normalized graph Laplacian

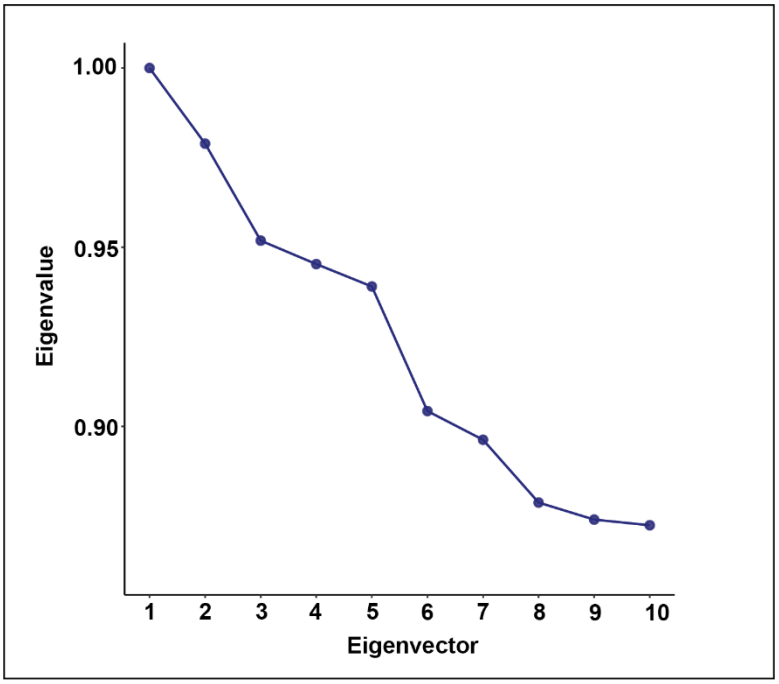

The eigenvalues of the eigenvectors from the graph Laplacian of the WMH probability maps of the study cohort, with the greatest eigengap between the fifth and sixth eigenvectors corresponding to the optimal number of clusters, k =5.

eFigure 5. Regression diagnostic plots for each data-driven WMH spatial pattern.

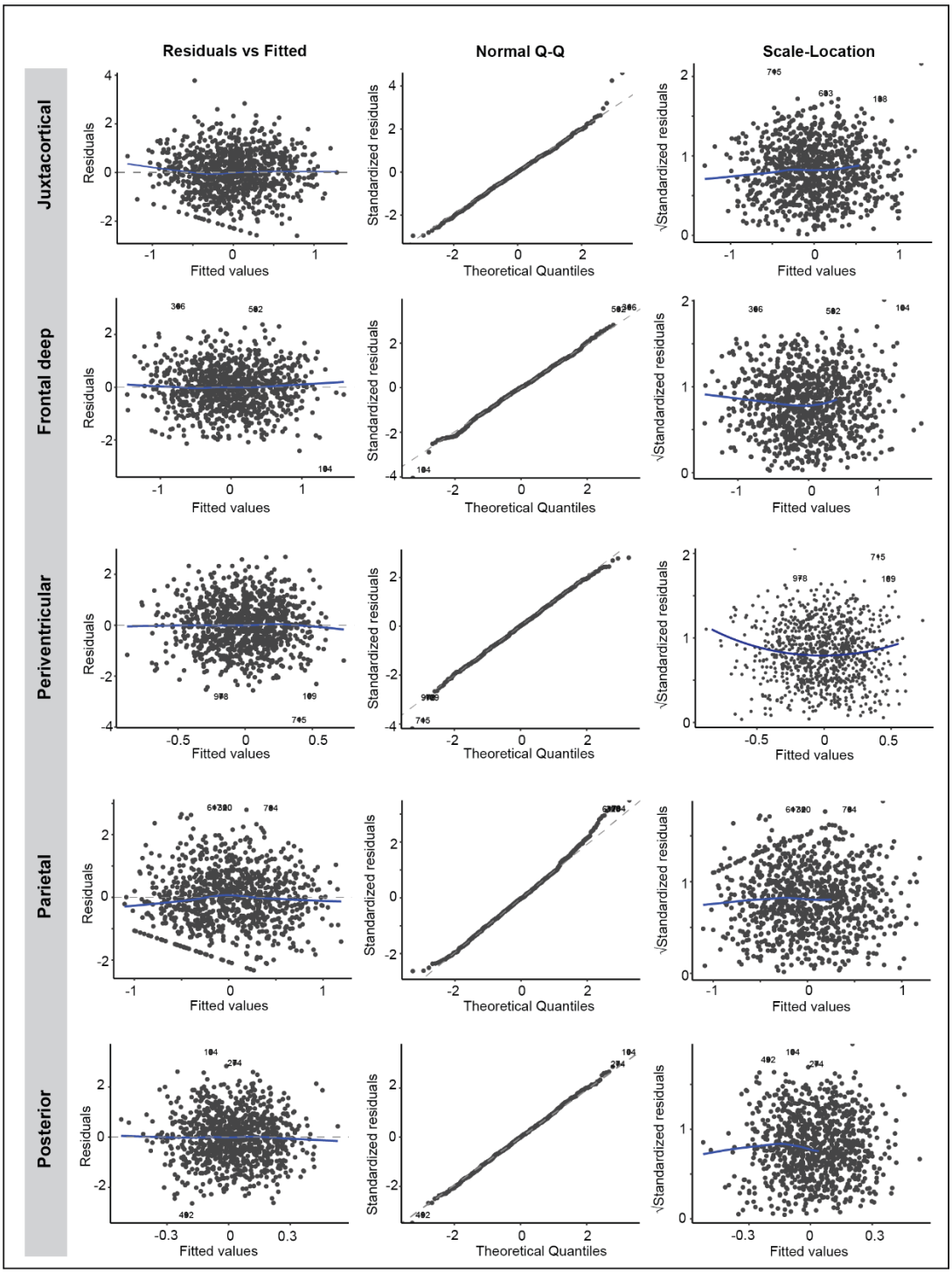

Assumptions of linear models including mean residuals =0, absence of correlation between residuals and dependent variables, normality of residuals, and homoscedascity of residual variance were fulfilled.

eFigure 6. Boxplot of global WMH burden as a function of cognitive status assessed by CDR.

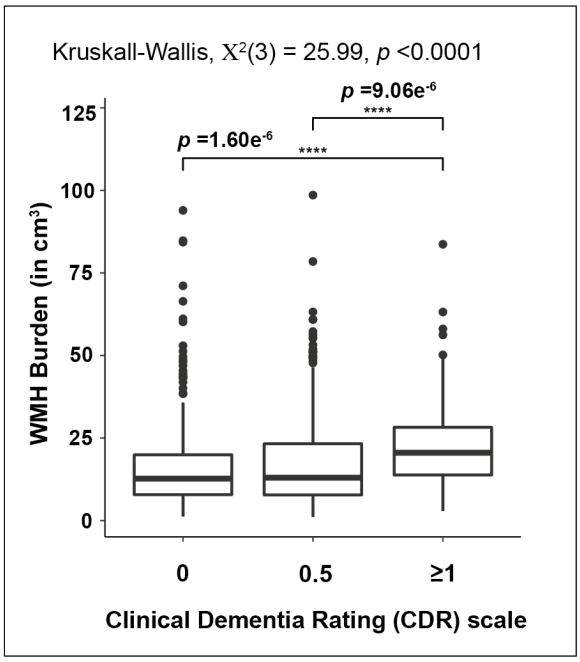

Higher global WMH burden is associated with greater risk of cognitive impairment. The central line, top and bottom edges of each box plot represent the median, 25th and 75th percentiles, respectively; error bars extend to the most extreme non-outlier data points; outliers are indicated by the symbol • .

eTable 1. MRI acquisition protocol parameters

Parameter	T1-weighted	FLAIR
In-plane matrix (pixels)	256 x 256	256 x 256
Slices, n	256	35
Thickness (mm)	1.2	5
In-plane resolution (mm)	1.0 x 1.0	0.8594 x 0.8594
Repetition time, TR (ms)	2300	9000
Echo time, TE (ms)	2.98	90 or 91
Flip angle	9.0	90 or 150
Pulse sequence	GR/IR	SE/IR

eTable 2. Comparison of the WMH segmentation performance between U-Net and UCD Four Tissue segmentation method on the ADNI test dataset (n=20).

	DL (U-Net)		UCD ADNI	
	mean	**95% CI**	**mean**	**95% CI**
Dice similarity coefficient	0.76	0.72 – 0.80	0.50	0.43 – 0.58
Volume difference	-0.13	-0.26 – -0.01	-0.51	-0.61 – -0.42
AUC-PR	0.86	0.82 – 0.89	0.69	0.66 – 0.73
H95 (mm)	11.2	5.97 – 16.35	18.95	16.11 – 21.78
AVD	25.27	17.33 – 33.21	51.51	42.53 – 60.50
Recall	0.54	0.47 – 0.61	0.22	0.18 – 0.27
F1	0.60	0.56 – 0.65	0.31	0.27 – 0.35

Mean and 95% confidence intervals for each individual performance metric. Metrics include: (1) Dice similarity coefficient (DSC), (2) volume difference (VD) between the automated schemes and manual segmentations, (3) area under the curve of precision-recall (AUC-PR), (4) modified Hausdorff distance (95^{th} percentile; H95), (5) absolute of the percentage volume difference (AVD), (6) sensitivity for detecting individual lesions (Recall), (7) F1-score for individual lesions (F1).

eTable 3. Mean values of the Dice Similarity Coefficient (DSC) and area under the curve of precision-recall (AUC-PR) for U-Net and UCD Four Tissue automated segmentation schemes for the test dataset grouped by WMH burden.

	DSC				AUC-PR			
	S	**M**	**L**	**VL**	**S**	**M**	**L**	**VL**
U-Net	**0.74**	**0.80**	**0.79**	**0.72**	**0.89**	**0.92**	**0.85**	**0.81**
UCD ADNI	0.30	0.50	0.50	0.60	0.62	0.70	0.68	0.72

S, Small; M, Medium; L, Large; VL, Very Large

DSC and AUC-PR values closer to 1 indicate higher segmentation accuracy.

Bolded values indicate the best scores.

eTable 4. Framingham Risk Score-based scoring scheme for hypertension combining average systolic blood pressure and antihypertensive medication use.

HTN-S	Untreated SBP (mmHg)	Treated SBP (mmHg)	n, (%)
0	97-105	97-105	13 (1.2)
1	106-115	106-112	49 (4.7)
2	116-125	113-117	154 (14.7)
3	126-135	118-123	219 (20.9)
4	136-145	124-129	188 (17.9)
5	146-155	130-135	142 (13.6)
6	156-165	136-142	121 (11.6)
7	166-175	143-150	97 (9.3)
8	176-185	151-161	44 (4.2)
9	186-195	162-176	17 (1.6)
10	196-205	177-205	2 (0.2)

Abbreviations: **HTN-S**, composite hypertension score; **SBP**, average systolic blood pressure

eTable 5. ADNI image IDs (baseline 2D-FLAIR MRI) of the study participants (n=1,046).

180309	296364	284416	294214	372414	242275	376931	255390	206878	290876	274159	401255	287884	281968	377861	342520
191815	297785	287475	293780	384980	243801	385102	260215	206472	296451	313901	396276	295451	285330	383430	257188
192252	300194	294282	292442	207518	245679	389315	260731	213723	293378	315251	208717	294883	290380	179557	257204
192471	302853	293941	294944	241004	272346	401128	261213	224106	296086	331953	295897	295493	348827	181148	264486
196076	303724	296249	305879	250352	291470	245498	261238	261787	293923	385349	319230	310724	217886	180182	266835
202161	304661	328201	303058	250370	280955	243897	267428	270662	298613	394663	325970	316179	289657	183861	269639
205393	304676	376234	310316	254358	291475	321557	266885	275316	301504	253076	341502	322970	298264	190935	281455
205612	304743	383462	325640	255555	315163	323233	268149	284801	307196	253092	342317	339518	300840	191600	285101
207344	306378	207374	325680	274947	312748	326211	274542	286310	308778	252070	361964	376426	361366	192073	287515
207602	306471	235705	337688	294419	375880	374726	283902	288989	310624	359739	356509	203118	341825	199270	286216
208262	306883	267168	337798	299189	237739	395044	285075	290857	311826	374924	247530	201037	362411	202690	297495
208842	307552	265544	339509	324274	238490	399778	286564	299035	310919	378413	289338	207363	362426	205441	291076
220049	311924	270647	349053	352569	270464	194189	290675	241613	315674	382637	290816	209979	364797	209237	295416
220068	313856	271893	360437	388960	274485	205880	304868	277489	358222	192782	306673	214765	365273	222053	301111
223897	314030	284911	348598	205086	281770	206071	305335	280053	378125	206270	316523	215760	368417	285761	301667
223991	315849	287801	361225	207828	288317	217800	314310	350944	223083	208015	357483	247634	387093	289724	297488
224717	316442	289789	385055	208690	297184	219906	307695	378547	228516	207230	375694	253731	387123	308310	301627
225330	318414	294232	199196	224441	303279	237446	308456	214099	240969	278817	642389	239634	284991	267721	348494
226180	318504	310563	202428	306177	302649	243485	312896	225665	255892	279471	722970	240499	315768	281039	358778
226191	319413	313894	207987	308640	306975	245738	315945	235316	261795	281599	733883	243627	336746	282551	368290
227598	319421	333679	262081	317194	316724	255155	338191	241698	267416	281888	738295	265066	345637	283795	374292
228466	319540	338124	268931	316465	321501	254864	339729	252719	268466	283263	742009	269619	193011	299141	381304
228829	321384	351489	266630	324945	323102	262831	342676	252807	269452	283877	755669	289476	232432	300820	381464
233361	322005	355095	272224	322871	340469	307592	365432	254252	272197	284864	759974	291666	239352	302240	367564
233427	324341	364861	273500	330089	355514	309825	359038	252817	232234	285811	783530	294333	247484	306288	367758
234461	325741	367587	290300	336137	371191	318811	376069	253240	240903	286752	791893	300630	253441	321424	260980
235259	326452	372557	301396	336331	367197	336272	377337	264962	256755	287210	339122	180260	252944	322423	262536
238624	331754	381176	306075	336921	376439	369896	193104	280154	259334	287646	368155	190002	253494	376024	265905
240511	332651	381390	311902	335352	382228	372775	196356	280669	259686	287996	191959	216945	282070	380760	270415
240806	336548	247203	323222	338749	384060	376805	217599	285463	267902	289562	193795	240948	265473	207318	278383
240932	341978	282007	360316	338557	387293	202821	241099	296143	267710	291319	261197	243558	280810	207970	282256
241968	342266	283909	382188	338861	197862	204973	253471	295321	279111	292387	269926	246001	291862	252153	288827
242124	342849	375333	384818	339873	218399	205389	257378	307567	279178	293619	280123	267944	288464	254318	291129
243333	344146	215806	385126	359294	228846	207425	261716	321278	282289	374428	281551	293335	325911	255087	297161
243785	346240	239729	258952	360921	254993	205379	265933	322559	291233	247415	385978	283606	337126	262225	298462
243904	346705	244972	260910	361526	255505	209510	273683	191060	293630	251999	389088	311965	342334	283518	300799
244111	346809	244897	261990	364435	262517	223578	343521	228736	295966	254920	209606	311945	341788	291525	304633
245973	347640	256858	269276	363813	285683	223875	372741	248589	300036	260438	216305	335151	342273	307352	304623
246591	348331	258010	280786	364901	279142	239364	373609	253061	314335	266608	208298	248771	342913	295593	320492
247515	349856	260770	286480	365831	273578	239376	385775	269086	323158	268980	229407	258845	347405	307102	336504

247612	351431	314040	300339	373607	282043	310352	346345	357655	293999	268920	492607	337381	195224	281147	363766
248519	354659	316080	300531	373633	302746	316769	365350	361467	308397	269255	499410	330025	208294	282641	362831
249405	355057	332725	343915	375828	315483	316751	382715	368756	308421	269293	501930	339627	213359	290640	366046
249531	364688	330060	345552	386394	333836	330370	384476	374501	330234	271000	503734	360327	235154	339438	367902
250141	364842	325979	373544	390932	368793	335510	384351	375923	342483	274152	504915	368200	241326	194938	372458
250171	365081	335366	379091	234691	369971	342696	256892	377874	375503	274468	561266	374974	255991	209407	376124
250898	366682	206405	298381	250989	379903	274500	242724	353208	264204	274613	576766	208094	282443	261817	379853
251174	371616	206427	334255	265983	228293	283093	251121	354642	281015	277122	585818	217968	267458	262775	335403
251350	372847	228228	368627	260424	228299	322078	261523	307122	240919	278498	594652	238749	269152	267559	343040
251755	373241	238536	376769	267605	237032	330205	261842	321565	245779	278517	600812	237560	267881	272394	396299
253763	374427	243879	192500	265018	237204	360587	261500	321118	252867	254387	196567	251130	221795	317480	192264
254152	375946	248232	193916	274001	241386	372704	279076	381824	259916	257896	203628	251185	224604	332570	192464
254584	378488	255324	196685	285579	238385	379374	283443	212299	269840	270719	206904	263963	228784	340330	192828
254894	379750	290410	196584	298530	241374	302277	283575	224920	268049	270675	239980	269340	238610	195027	195818
255623	379985	296879	199170	300891	246548	304229	284892	236771	269041	276967	242229	293975	237085	199315	199332
256142	380900	297691	201117	368842	247652	305584	286235	255575	275237	274685	243000	316811	256182	240231	201269
257272	381333	319136	217736	377895	257473	312392	291210	258047	294081	278355	252238	382463	255840	245817	222943
257480	386338	343910	257577	373671	260504	313291	295573	273817	307650	282505	258437	384015	261465	247610	239297
257761	395526	363550	258065	378234	272573	318610	302940	273510	366199	284730	259938	192343	286985	250184	241294
258444	395977	372897	260042	183881	273196	348753	309927	277020	287129	285369	282211	235792	190795	251348	245968
258530	399738	376800	266171	181504	282633	189453	333551	279131	297886	324107	341291	481471	300084	374571	255313
258601	401703	381907	271931	184539	284329	185623	192492	303834	305200	329967	360355	487157	308183	378478	255976
259656	401704	225060	273248	208976	284314	189821	193310	312261	321226	340184	360656	487985	320435	378459	280370
259735	401925	241660	273563	229150	260585	404527	278363	307150	234920	264500	422062	300055	372713	255280	266128
259795	401998	261165	287526	228871	261330	411281	296780	331253	235231	415226	296868	361894	249145	266820	266211
260521	403657	264415	297536	229504	262286										

eTable 6. Overlap between the data-driven WMH spatial patterns calculated from repeated clustering experiments with bootstrap resampling of the full dataset (n=1,046)

WMH Spatial Patterns	Juxtacortical		Deep Frontal		Periventricular		Parietal		Posterior	
	mean	SD	mean	SD	mean	SD	mean	SD	mean	SD
Dice similarity coefficient	0.904	0.047	0.956	0.016	0.872	0.063	0.831	0.146	0.850	0.168

Mean and SD of the Dice similarity coefficient, DSC were calculated over ten repeated clustering experiments. DSC values closer to 1 indicate higher similarity.

eTable 7. Multiple regression models for WMH spatial patterns associations with CVSD and AD risk factors, adjusted for CDR at time of imaging (n=930)

	Juxtacortical		Deep Frontal		Periventricular		Parietal		Posterior	
	β	*p*	β	*p*	β	*p*	β	*p*	β	*p*
age	**0.04**	**$2.0e^{-16}$***	**0.06**	**$2.0e^{-16}$***	**-0.02**	**$6.9e^{-5}$***	**0.05**	**$2.0e^{-16}$***	**0.01**	**$3.2e^{-3}$***
sex (male)	**-0.48**	**$3.6e^{-15}$***	**-0.28**	**$8.7e^{-7}$***	**-0.17**	**$8.7e^{-3}$***	-0.06	0.32	-0.08	0.23
race (White)	-0.09	0.63	-0.06	0.76	0.02	0.93	-0.29	0.16	-0.07	0.76
race (Black)	-0.37	0.15	-0.11	0.63	-0.01	0.96	0.01	0.97	-0.01	0.98
hypertension$^{\alpha}$	0.05	0.03	**0.06**	**$2.1e^{-5}$***	-0.04	0.02	$-1.2e^{-3}$	0.94	-0.04	0.03
diabetes mellitus	0.18	0.06	0.23	0.01	-0.01	0.92	0.14	0.14	0.07	0.52
smoking	$7.3e^{-3}$	0.90	$1.1e^{-3}$	0.98	-0.07	0.27	0.07	0.28	0.07	0.28
alcohol use	-0.05	0.73	0.05	0.73	-0.02	0.93	-0.11	0.45	-0.11	0.52
cardiovascular disease	-0.06	0.49	-0.03	0.75	0.06	0.53	-0.05	0.59	-0.11	0.35
atrial fibrillation	-0.01	0.96	-0.03	0.85	$1.8e^{-3}$	0.92	0.04	0.79	0.10	0.56
hyperlipidemia	0.04	0.55	0.11	0.05	-0.06	0.39	-0.03	0.63	0.03	0.68
probable CAA	**0.37**	**$5.6e^{-4}$***	0.11	0.27	-0.24	0.04	0.28	0.01	-0.07	0.55
APOE ε4 allele	0.10	0.38	-0.23	0.04	0.27	0.03	0.03	0.79	0.15	0.24
APOE ε2 allele	0.19	0.83	-0.63	0.47	0.49	0.62	-0.65	0.48	-0.03	0.96
amyloid SUVR	0.34	0.03	0.15	0.30	-0.15	0.37	**0.49**	**$1.5e^{-3}$***	-0.03	0.85
CDR 0.5	0.10	0.15	**0.21**	**$8.2e^{-4}$***	-0.09	0.21	-0.02	0.75	-0.10	0.19
CDR ≥1	**0.32**	**$6.4e^{-3}$***	**0.59**	**$1.2e^{-7}$***	-0.28	0.03	**0.35**	**$3.0e^{-3}$***	0.14	0.28

Linear regression models were used independently for each WMH spatial pattern, using all risk factors jointly as predictors and relative WMH burden for each WMH spatial pattern as outcome.

*significance (**bold**) at Bonferroni-corrected level $p<0.01$.

α composite hypertension score

Abbreviations: **CAA**, cerebral amyloid angiopathy; **SUVR**, standardized uptake value ratio; **CDR**, clinical dementia rating scale; **CSVD**, cerebral small vessel disease; **WMH**, white matter hyperintensities; β, beta-coefficient.

eTable 8. Associations between individually-modelled CSVD and AD risk factor interactions, on WMH spatial patterns.

CSVD and AD risk factors	Juxtacortical		Deep Frontal		Periventricular		Parietal		Posterior	
	β	*p*	β	*p*	β	*p*	β	*p*	β	*p*
HTN-S * probable CAA	-0.06	0.25	-0.06	0.19	$-3.5e^{-3}$	0.95	-0.01	0.77	-0.04	0.44
HTN-S * diabetes mellitus	-0.02	0.73	-0.05	0.33	-0.03	0.58	-0.02	0.65	0.11	0.04
HTN-S * amyloid SUVR	0.03	0.66	-0.08	0.21	0.13	0.07	-0.14	0.04	-0.04	0.54

Standardized betas (β) and *p* values are reported from regression models where each pair of CSVD and AD risk factor interaction are individually regressed onto WMH spatial pattern measures, covarying for age, sex, race, vascular risk factors (HTN-S, diabetes mellitus, smoking, alcohol use, cardiovascular disease, atrial fibrillation, hyperlipidemia), and amyloid-related risk factors (probable CAA, *APOE* genotype, amyloid SUVR).

Abbreviations: **CSVD**, cerebral small vessel disease; **HTN-S**, composite hypertension score; **CAA**, cerebral amyloid angiopathy; **SUVR**, standardized uptake value ratio.

eTable 9. Associations between the data-driven WMH spatial patterns and cognitive status assessment scores, adjusted for years of education.

	Juxtacortical		Deep Frontal		Periventricular		Parietal		Posterior	
	β	*p*	β	*p*	β	*p*	β	*p*	β	*p*
age	**0.04**	**$1.1e^{-15}$***	**0.06**	**$2.0e^{-16}$***	**-0.02**	**$1.7e^{-4}$***	**0.05**	**$2.0e^{-16}$***	**0.01**	**$8.3e^{-3}$***
sex (male)	**-0.45**	**$9.0e^{-13}$***	**-0.29**	**$1.0e^{-6}$***	**-0.20**	**$3.1e^{-3}$***	-0.02	0.71	-0.04	0.58
race (White)	-0.11	0.61	-0.06	0.77	0.03	0.90	-0.30	0.15	-0.08	0.72
race (Black)	-0.39	0.12	-0.11	0.64	0.01	0.98	-0.02	0.94	-0.04	0.89
hypertension$^{\alpha}$	0.05	0.04	**0.06**	**$1.9e^{-5}$***	-0.04	0.02	$-2.5e^{-3}$	0.87	-0.04	0.03
diabetes mellitus	0.17	0.07	0.23	0.01	$-1.5e^{-3}$	0.99	0.13	0.17	0.06	0.60
smoking	$-1.1e^{-3}$	0.99	$3.1e^{-3}$	0.96	-0.07	0.32	0.06	0.36	0.06	0.35
alcohol use	-0.05	0.74	0.05	0.74	-0.02	0.92	-0.11	0.46	-0.11	0.54
cardiovascular disease	-0.07	0.42	-0.02	0.77	0.07	0.48	-0.06	0.50	-0.13	0.19
atrial fibrillation	0.02	0.92	-0.03	0.82	-0.04	0.82	0.07	0.66	0.14	0.45
hyperlipidemia	0.03	0.62	0.11	0.05	-0.05	0.43	-0.04	0.54	0.02	0.78
probable CAA	**0.36**	**$9.4e^{-4}$***	0.11	0.25	-0.23	0.05	0.26	0.02	-0.09	0.45
APOE ε4 allele	0.10	0.40	-0.23	0.04	0.27	0.03	0.03	0.82	0.15	0.25
APOE ε2 allele	0.21	0.82	-0.63	0.47	0.49	0.62	-0.64	0.49	-0.02	0.99
amyloid SUVR	0.34	0.03	0.15	0.30	-0.15	0.37	**0.49**	**$1.5e^{-3}$***	-0.03	0.85
CDR 0.5	0.09	0.20	**0.22**	**$7.3e^{-4}$***	-0.08	0.27	-0.03	0.61	-0.11	0.13
CDR ≥1	0.29	0.01	**0.60**	**$1.0e^{-7}$***	-0.26	0.05	**0.31**	**$8.2e^{-3}$***	0.10	0.46
education	-0.02	0.04	$5.5e^{-3}$	0.61	0.02	0.10	-0.03	0.02	-0.03	0.01

Linear regression models were used independently for each WMH spatial pattern, using CDR group categories jointly as predictors (CDR =0.5, CDR ≥1) versus normal cognition (CDR =0) and relative WMH burden as outcome. Models were adjusted for age, sex, race, amyloid-related and vascular risk factors. Years of education was included as additional confounder and marker of brain resilience. The pattern of associations between regional relative WMH burden and cognitive impairment was unchanged except for nominal significance (β=0.29, *p*=0.01) for the juxtacortical region.

*significance (**bold**) at Bonferroni-corrected level *p*<0.01.

α composite hypertension score

Abbreviations: **CAA**, cerebral amyloid angiopathy; **SUVR**, standardized uptake value ratio; **CDR**, clinical dementia rating scale; **CSVD**, cerebral small vessel disease; **WMH**, white matter hyperintensities; β, beta-coefficient